Title

Strong O 2p–Fe 3d Hybridization Observed in Solution-Grown Hematite Films by Soft X-ray Spectroscopies

Journal

The Journal of Physical Chemistry B, 122(2)

ISSN

1520-6106

Authors

Ye, Yifan
Thorne, James E
Wu, Cheng Hao
et al.

Publication Date

2018-01-18

DOI

10.1021/acs.jpcb.7b06989

Peer reviewed

Strong O 2p-Fe 3d Hybridization Observed in Solution-Grown Hematite Films by Soft X-ray Spectroscopies

Yifan Ye[1], James Thorne[2], Cheng Hao Wu[1], Yi-Sheng Liu[1], Chun Du[2], Ji-Wook Jang[2], Erik Liu[2], Dunwei Wang[1], and Jinghua Guo[1,3]*

1. Advanced Light Source, Lawrence Berkeley National Laboratory, Berkeley, CA 94720, USA

2. Department of Chemistry, Merkert Chemistry Center, Boston College, Chestnut Hill, Massachusetts 02467, USA

3. Department of Chemistry and Biochemistry, University of California, Santa Cruz, CA 95064, USA

~~Abstract~~ABSTRACT:

Photoelectrochemical (PEC) water splitting holds the potential as a direct route for solar energy conversation and storage. The performance of a PEC device is strongly influenced by the electronic properties of the photonanode surface. It has been shown that the synthesis methods can have profound impact on the electronic properties and PEC performance of various photo-electrode materials such as hematite. In this work, soft X-ray spectroscopic techniques, including O K-edge XAS, and Fe L-edge XAS/XES, have been employed to investigate how the synthesis methods impact the electronic structure of resulting hematite materials. It is found that the hematite samples via solution regrowth methods show dramatically increased 3d-4sp band ratios in O K-edge XAS spectra and decreased relative elastic peak intensities in Fe L-edge RIXS spectra compared to samples synthesized via ALD or solution grown. The difference observed in O-K and Fe-L spectra indicated that solution regrowth strategy alters the O 2p-Fe 3d hybridization and hence the electronic structure of the hematite films, which proves to be beneficial for PEC performance of the hematite photoanode. Our findings provided new insights and potentially useful strategies for enhancing the PEC performance of photoanode materials.

~~Introduction~~INTRODUCTION:

In the quest to reduce human's environmental footprint, it has become more crucial than ever to develop new and sustainable green energy technologies. Among the emerging energy technologies, photocatalysis deserves special attention, considering the vast abundance of solar light. Solar water splitting, one of the most important applications of photocatalysis, holds great promise for energy conversion and storage.[1-3] To achieve efficient and inexpensive PEC water splitting, finding the photo-catalyst materials with suitable electronic properties is the key but remains a challenge even after decades of intense research. [4-5] [6-10] Among the myriad of available materials, metal oxides, particularly the 3d transition metal oxides (TMOs), have established their prominence in this field due to their stability, cost-efficiency, and the tunability of their electronic characteristics.[11-13] Hematite is a prototypical photoanode material with a favorable band structure and high stability and thus has attracted intense attention.[14] However, hematite has not delivered its expected performance, as it typically shows small photovoltages and poor catalytic activity for the OER.[15-17] Therefore, these challenges must be investigated and understood in order to enhance the PEC performance of hematite materials.

Suitable surface/interface treatment can passivate deleterious surface states and reduce effects such as surface Fermi level pinning and therefore has been regarded as an effective method to improve the water splitting performance.[18-20] For example, the effectiveness of the surface modification by loading OER catalysts on the photoanode surface has been demonstrated in numerous studies, such as Co-Pi on bismuth vanadate, and $NiFeO_x$ on hematite.[20-21] Inspired by this approach, Ji-Wook et al., developed a solution regrowth strategy where additional hematite layers were deposited onto the original hematite films via a few regrowth cycles inside the growth solution. This regrowth strategies proves to be effective to reduce the surface states on hematite films and thus improves the photovoltages by 27%. With the addition of the $NiFeO_x$ catalyst onto the regrown hematite surface, the photovoltage is further improved to a value of 0.8 V, the highest reported photovoltage for hematite to date. This facile regrowth method holds great promise in the optimization of other PEC systems and a better understanding on the mechanism for performance improvement would be helpful for the adaptation in other systems. Several characterization techniques have been employed to study the surface morphology and surface kinetics of hematite photoanode before and after the regrowth process.[22] The impact of the growth methods on the electronic structures is another piece of useful information to better understand the improvement mechanism.

X-ray spectroscopies are a series of powerful techniques to probe the electronic structure of materials.[23-24] X-ray absorption spectroscopy (XAS) and X-ray emission spectroscopy (XES) are commonly employed to study condensed-matter materials by probing element specific transitions from either the core level to conduction band or from the valence band to the core level, respectively.[25-27] The 3d TMOs have been extensively investigated by XAS and XES. Since oxygen has an electron configuration of $1s^2 2s^2 2p^6$ in a purely ionic model, the transition from O1s to 2p is prohibited due to the fully occupied 2p orbital. However, the 3d TMOs are not fully ionic, and the considerably more covalent bond reduces the number of filled states of O 2p orbital. Therefore, the peak intensities in the O K-edge XAS spectra are strongly correlated with the covalency in the TMO bond, especially for the peaks resulting from O 2p – Fe 3d hybridizations.[28] The TM L-edge can also be probed, where the XAS measures the transition from 2p to 3d orbital, which represents the state of the valence electrons in TMOs. Resonant inelastic X-ray emission spectroscopy (RIXS) and non-resonant X-ray emission spectroscopy (Nr-XES) use resonant and non-resonant excitation energy, respectively, to excite the core electrons in the materials. X-ray spectroscopic techniques have previously been employed to investigate various hematite systems, including size and shape effect on the electronic structures in the hematite systems and hematite-TiO_2 heterojunction systems,[29-31] from which detailed understanding of the XAS and XES transitions for hematite has been established. In this work, we aim to use x-ray spectroscopies to reveal how the growth methods impact the electronic structures of hematite materials and its correlation with PEC performance.

~~Experimental~~EXPERIMENTAL:

The hematite films characterized here were synthesized via two different methods, i.e., atomic layer deposition (ALD) and solution-based regrowth methods. The ALD samples were obtained via reactions by alternating pulses of iron precursors (iron tert-butoxide, heated to 125 °C) and water (kept at 25 °C), both delivered in N_2 carrier gas at a rate of 10 ml/min. 500 ALD cycles were used to produce the pre-formed iron oxide films, which then went through a

high-temperature annealing step to ensure the complete conversion to crystalized hematite films. The pre-formed ALD films annealed at 500 and 800 °C are denoted as ALD 500 and ALD 800, respectively.

Solution-derived samples are synthesized in the solution containing 0.15 M iron (III) chloride hexahydrate ($FeCl_3$, 97%, Alfa Aesar) and 1 M sodium nitrate ($NaNO_3$, 99%, Alfa Aesar) at 100 °C for 1 hr. The as-synthesized FeOOH films were further converted to Fe_2O_3 film by thermal annealing at 800 °C for 5 mins. The sample obtained with this method is named as sdH (solution-derived Hematite). To obtain the solution-regrowth hematite (rgH I) samples, the sdH films were further immersed ~~the sdH sample~~ in the above-mentioned solution at 100 °C for 1 hr and then annealed again at 800°C for 5 mins. Additional one and two cycles of reaction-annealing process were applied to the sample labeled as rgH II and rgH III, respectively. The thickness of the hematite films varies as a function of the growth method, which was summarized in Table S1 in the supporting information. Among all six samples, rgH II showed the highest photovoltage and lowest turn-on voltage in PEC measurements, as shown in the Figure S1.

The X-ray spectroscopies measurements are performed on beamline 8.0.1 at the Advanced Light Source, Lawrence Berkeley National Laboratory. The photon energy resolution was set to be 0.1, 0.2 and 0.5 eV for O K-edge XAS, Fe L-edge XAS, and Fe L-edge XES, respectively. TEY and TFY signals were recorded simultaneously in XAS measurements, providing surface and bulk sensitive characterizations, respectively. TEY signals were recorded by monitoring the sample drain current, whereas TFY signals were collected using a channeltron detector. XES spectra were acquired using a grazing-incidence grating spectrometer.

Both TEY and TFY XAS spectra were normalized to the incoming photon flux, represented by drain current measured from an upstream gold mesh. A linear background based on the slop in the pre-edge region was subtracted from each flux-normalized XAS spectra, which was then normalized again to the post-edge region. The XES spectra were normalized to the high-energy region. Quantitative deconvolution of spectra was performed by using software Athena Demeter version 0.9.24.

As shown, with gray lines in Figure 1, the individual absorption events contributing to a XAS spectrum were fit in order to separate the hematite signal from the substrate signal in a quantitative fashion. After subtracting an arctangent background, several Gaussian functions, corresponding to signals from both the hematite films and FTO substrate, were employed to fit the XAS spectrum.

~~Results~~ RESULTS and ~~discussion~~DISCUSSION:

Figure 1 shows both TFY and TEY XAS spectra of hematite films obtained via different methods. All spectra can be divided two regions: the O2p-Fe3d hybridization region (528-534 eV) and O2p-Fe4s4p hybridization region (534-546 eV). In the O2p-Fe3d region, two well-resolved peaks are originated from the t_{2g}/e_g splitting from crystal field effect.[27, 29] Because the inelastic mean free path for fluorescence photons (few hundred nm) are much larger than that of secondary electrons (few nm), TFY spectra, as well as XES spectra, are typically considered bulk-sensitive while TEY spectra are more surface sensitive. For each sample, TEY and TFY spectra are substantially different, which can be better visualized in the overlayed spectra shown in Figure S1. The most prominent difference is the ratio of the peaks in the two regions ~~significantly~~. Among these six samples, the TEY spectra are quite similar and in line

with the previous reported hematite spectra, further confirming that the measured films synthesized by ALD method and solution based method are indeed pure hematite films.[10] The TFY spectra, however, show an additional peak located at 533.8 eV for samples ALD-500, ALD800, sdH, and rgH1. This feature could correspond to the signal from the FTO substrate [27] or the impurities in the film bulk. Given the fact that this addition peak decrease with film thickness (from sample ALD-500 to rgH I), we can rule out the contribution from bulk impurities, which should be independent of the film thickness. The O K-edge XAS signal from the substrate has also been displayed in the Figure S2. Such interference from the substrate is not present in the spectra of thick samples (rgH II and rgH III), but their TEY and TFY spectra still show substantial difference, suggesting that there are differences in the surface and bulk electronic structures of the solution samples.

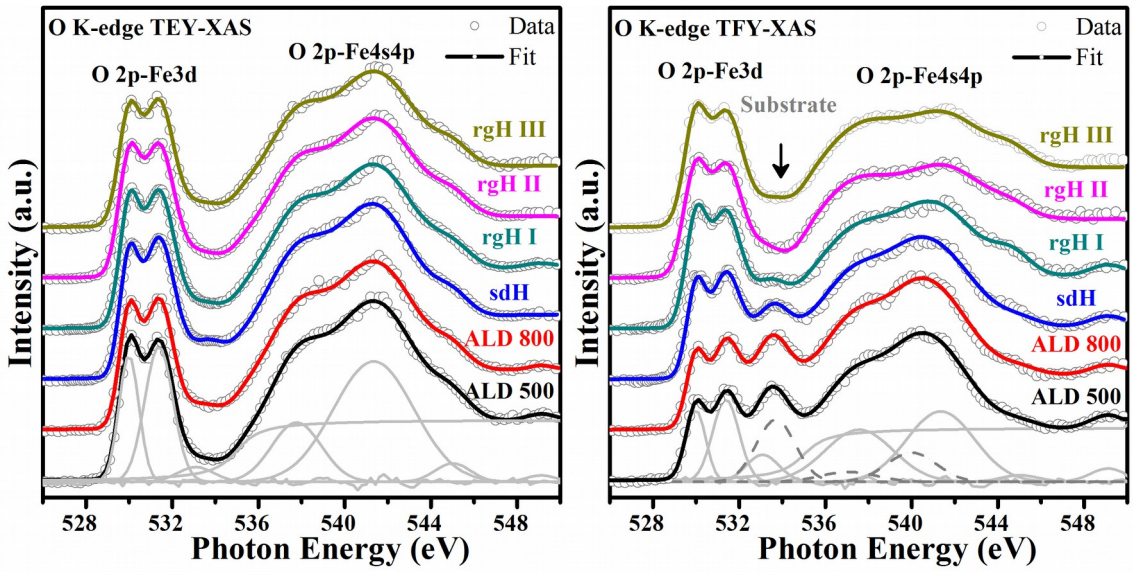

Figure 1: O K-edge XAS signals of Hematite films synthesized by different methods, the peak decomposition has also indicated in the figure. The experimental data is shown with the open circles and the fitted results are shown with the solid line. The substrate signals are included to fit the TFY spectra and displayed by dash lines.

To further reveal more details in the electronic structural differences among the samples, the XAS spectra were analyzed by peak deconvolution, as shown in Figure 1, S4~~2~~, and ~~S3~~S5. Based on the peak fitting results, the 3d-4sp band ratios can be quantitatively compared among the six samples, as shown in Figure 2. For the two ALD samples, the band ratios in the surface (in black) and in the bulk (in red) are very close (the inset of Figure 2). This is because the ALD samples are thin enough to be fully detected under both TEY and TFY modes. A much larger difference between surface and bulk band ratios was observed for the solution-grown samples and the difference increase with numbers of regrowth cycles.

Extensive XAS/XES studies on various 3d TMOs suggested a quantitative linear relationship between the 3d-3sp band ratio and the number of 3d electrons: A higher 3d-4sp band ratio corresponds to fewer 3d electrons in the 3d TMOs, and vice versa.[23, 30, 32-33]

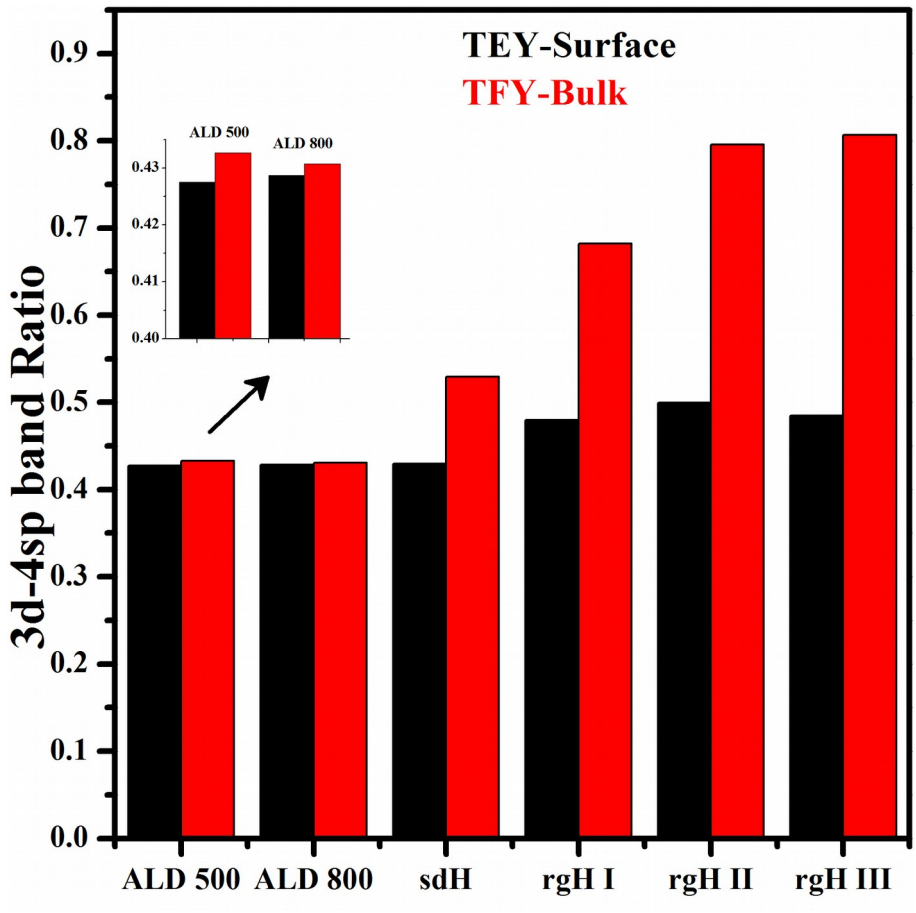

Figure 2: 3d-4sp band ratio of different hematite films obtaining from O K-edge XAS. Signals obtained from TEY and TFY detection modes have been denoted as surface-band ratio (black) and bulk-band ratio (red), respectively. For the two ALD samples, the surface- and bulk- band ratio values are close to each other and has been included in the inset of Figure 2.

According to the linear relationship reported in the literature, the band ratio of ~0.43 for the ALD samples corresponds to an average 3d electron number of 5.5,[23, 30] which is higher than the expected number of 5 in hematite. The sample sdH shows similar surface-band ratio in comparison with the ALD samples, while the bulk-band ratio is significantly higher. After the regrowth cycles, the samples rgH I, II, and II show a mild change in the surface band ratio whereas the bulk band ratio changes dramatically. The surface band ratios grows from 0.43 for sdH to 0.52 for rgH II, corresponding to 3d electron numbers from 5.5 to 5.1. As a comparison, the bulk band ratio increased from 0.54 for sdH to 0.78 for rgH II, corresponding to 3d electron numbers from 5 to 3.5.[23, 30] The abnormal d electron number indicates the complication that arises after the hybridization between Fe 3d, 4sp and O 2p.

To better understand the Fe-O hybridization, the Fe L-edge was further investigated. For these experiments only the TEY data were recorded, because TFY spectra were severely distorted due to self-absorption effect. As shown in Figure S6[4], the Fe L-edge TEY spectra appear very similar among all samples and resemble hematite spectra reported in the literature.[34] For quantitative comparison, the L_3 peak intensities in the normalized spectra are plotted in Figure 3. The intensities of L_3 peaks were calculated by integrating under L3-edge spectra preceded by

subtracting a linear background between 705 and 713 eV. [33] From sample ALD 500 to sample rgH II, the L3 peak intensity decreases continuously, but shows slight increase for the rgH III sample. The decrease in L3 intensity can be ascribed to the reduction of the density of the unoccupied states, indicating that more d states are filled. The trend shown in Figure 3 suggest that more electrons occupy the Fe 3d orbital in the solution-grown samples compared with the ALD samples and the first two regrowth cycles further increase the 3d electron numbers. This is in contrary to the conclusions derived from O K-edge TEY spectra, which suggest slightly fewer electrons occupying the 3d orbital with each regrowth, which will be discussed in more details later.

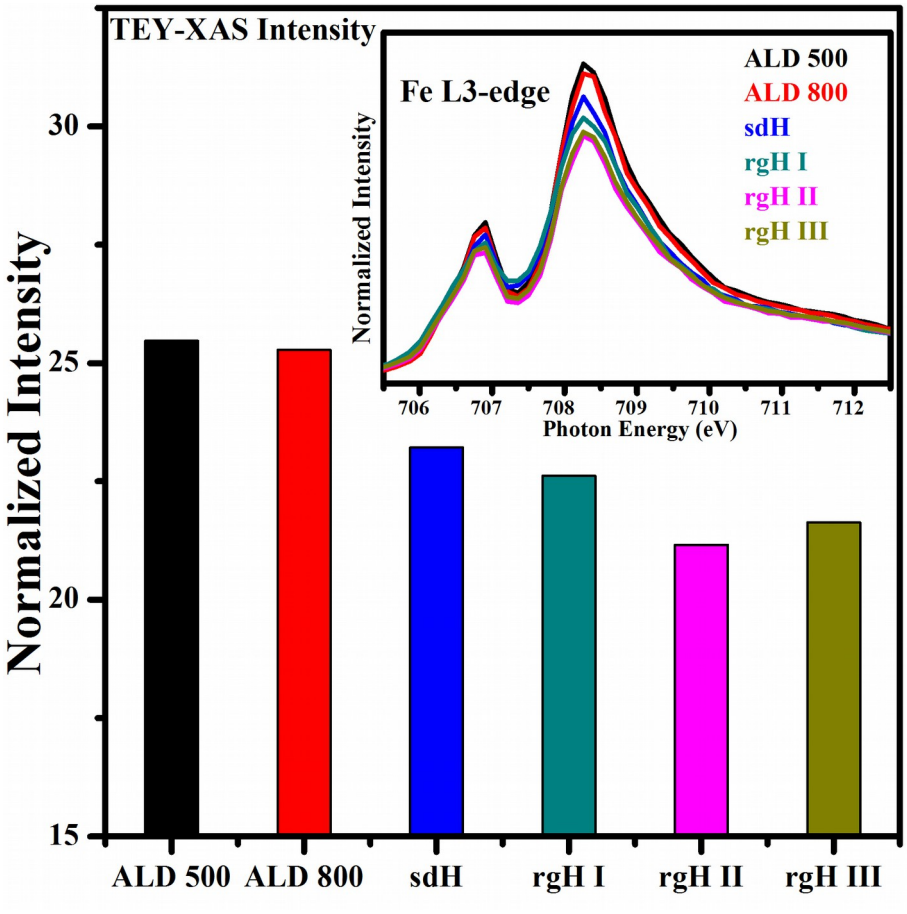

Figure 3: Fe L-edge TEY-XAS signals of the hematite films, the L3 edge has been enlarged to show a clear comparison.

Since the Fe 3d orbital is partially filled, to get a complete picture of Fe 3d configurations, it is necessary to investigate both the conduction band and valence band of hematite films. XAS spectra only provide information of the conduction band, XES techniques (including RIXS and Nr-XES), on the other hand, can provide insight to the valence band states. As has been well documented before, the relative intensity of the elastic peak in RIXS spectra is an indicator of the degree of localization of the valence electrons. The inset of Figure 4 shows two representative RIXS spectra of sample ALD 500, excited at t_{2g} and e_g peak energies, respectively. For relative peak intensity calculations, the inelastic peak was fitted with a Gaussian function (as shown in the inset of Figure 4 and Figure S5S7) and the relative intensities of the inelastic peaks for all the samples are plotted in Figure 4. The elastic peak ratios for solution-grown samples are smaller than the ALD samples, suggesting a more delocalized characteristic of

Fe 3d electrons in the solution samples.[35] The higher level of delocalization is most likely a results of stronger hybridization between O 2p and Fe 3d states, which leads to additional electrons transfer from the O site to the Fe site.[36] Such additional electron transfer between O and Fe can explain the opposite trends of 3d electron numbers deduced from O-K and Fe-L XAS spectra.

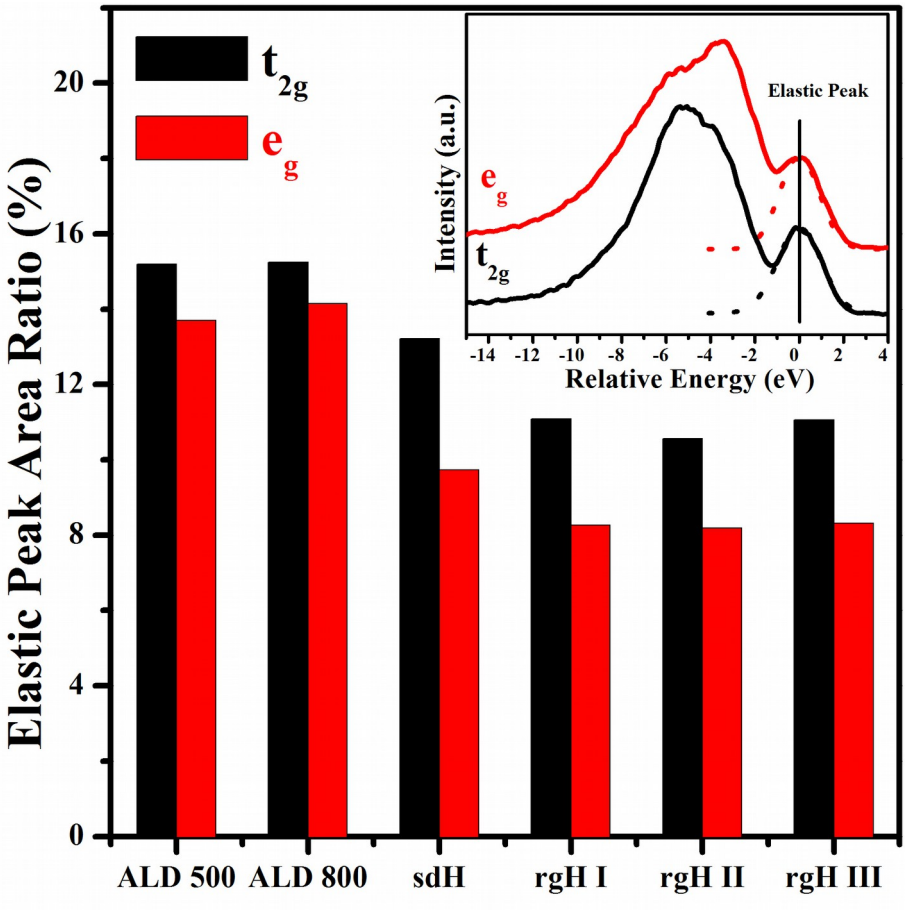

Figure 4: Elastic peak intensity ratio of Fe L-edge RIXS spectra excited at t_{2g} and e_g energies, the RIXS spectra of sample ALD 500 have been included as an inset, the fitted elastic peak region has been shown in a dash line.

In addition to the Fe L-edge RIXS data, the Nr-XES data were also investigated. As shown in representative Nr-XES spectra of ALD 500 in the inset of Figure 5 and spectra in the Figure S8, the two peaks represent the transitions from occupied 3d orbitals to $2p_{1/2}$ and $2p_{3/2}$ core levels, respectively. The branching ratio of $I(L_3)/I(L_2)$, summarized in Figure 5, provides another indicator for the difference in the electronic structure among these samples. The L_3/L_2 branching ratio of note that the branch ratio of solution samples appears substantially larger than that of ALD samples. It has been reported that the intensity ratio $I(L_3)/I(L_2)$ varies due to the occupancy of L_3 and L_2 levels, which depends on the chemical state of the probed elements. Such $I(L_3)/I(L_2)$ ratio of 3d transition metals and alloys is typically large owing to the non-radiative Coster-Kronig transition between L_2 and L_3,[37] and the probability of such transition is distinctly lower for 3d metal oxides because of the presence of an energy gap. The higher branching ratio of $I(L_3)/I(L_2)$ for solution-grown samples possibly suggests a smaller bandgap compared to the ALD samples. Samples rgH I and rgH II shows even higher branching ratios, indicating that the first two regrowth cycles

lead to a slightly decreased bandgap in the resulting hematite film. Such decreasing trend is reversed in the third regrowth cycle. The change in band gap is another strong indication of significant electronic structure change in solution-grown samples, which may also be due to the changes of the hybridization degree between O and Fe.

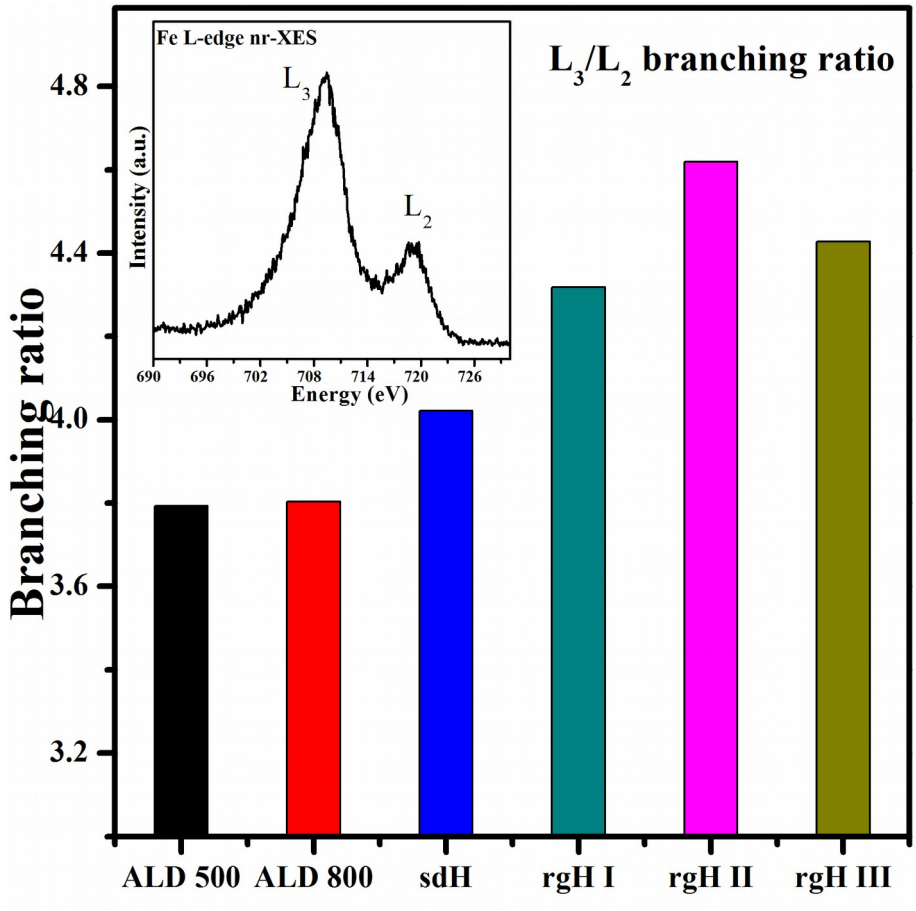

Figure 5: The L3/L2 branching ratio of Fe L-edge Nr-XES of various hematite samples, the Fe L-edge Nr-XES spectrum of ALD 500 has been displayed in the inset.

The comparison between the surface-sensitive TEY XAS spectra (both O-K and Fe-L) and the bulk-sensitive TFY XAS and XES/RIXS spectra suggests that the electronic structure difference is more prominent in the bulk than on the surface. The surface sensitive Fe L-edge XAS peaks showed mild intensity changes (around 10% variation among the spectra shown in Figure 3), similar to the level of intensity variation in the O K-edge TEY-XAS. On the other hand, the bulk sensitive Fe L-edge RIXS features showed much larger variations in intensity (around 50% variation among the spectra shown in Figure 4), also consistent with the large variations observed in the O K-edge TFY-XAS. These similarities between O-K and Fe-L spectra observed both in the bulk and on the surface of the hematite films further suggested the changes of the electronic structures across the entire film were influenced by both O and Fe sites as a results of stronger O2p-Fe3d hybridization.

As discussed in the previous section, the surface modification on photoanode surface has been proven to be an effective method to improve the PEC performance. One may claim that, in this work, the bulk electronic structure has been more affected than the surface by the regrowth method, which seems to suggest that the bulk electronic

structure changes is the driving factor for the performance enhancement. This is due to that the detection depth of the TEY signal is more surface sensitive than the electrode/electrolyte interfacial layer where PEC reactions take place. As well known, the photovoltage in hematite only develops within the space charge region, which is around 20-30 nm wide. The space charge region layer is thicker that the TEY detection depth (ca. 5-10nm) and within the region of the TFY detection depth (ca. hundreds nm). Therefore, the observed growth method induced changes of both the surface and bulk electronic structures are the driving factor for the performance enhancement.

The origin of the strong hybridization between O and Fe in solution-grown samples is still unclear, but may be connected to structure of the hematite films. According to the previously reported structural and electrochemical characterizations, the solution growth method produces hematite films with lower degree of surface disorder, which may be a contributing factor contributing for the suppression of hybridization. From all the X-ray spectroscopic data, the samples with the best PEC performance, rgH II, shows strongest O 2p- Fe 3d hybridization among all the samples. It is possibly because strong hybridization between the cation sites and O anion sites can facilitate the charge injection/extraction on the electrode surface during the electro-catalytic reaction. Such electronic structure-performance correlation suggests that the significant impact of the occupancy of the Fe 3d orbitals and the O 2p- Fe 3d hybridization on the electronic properties of the hematite materials and their PEC performance in water splitting reactions,[33] providing new insights and possible strategies for the performance enhancement of photoanode materials for PEC water splitting reactions.

~~Conclusion~~CONCLUSIONS:

The hematite films synthesized by ALD method and solution-derived growth method have been investigated using X-ray spectroscopies. Analysis of XAS and XES/RIXS spectra revealed that performance ~~improved~~ improvement observed in regrown solution samples is possibly related to a stronger hybridization between O 2p-Fe 3d hybridization. The hybridization level increases with each regrowth cycle~~, and it maximizes~~ until maximizing after the second cycles and then decreases with further regrowth. The stronger hybridization between the cation sites with O enhances the capability of the oxygen electro-catalysis, providing useful information to understand the mechanism of improvement in the PEC performance. This study indicates that the solution regrowth method can not only alter the morphological structure but also change the intrinsic electronic structure of the materials, establishing a possibility of a broad application of this strategy in materials synthesis. This work also illustrated the capability of synchrotron X-ray technique to provide unique information regarding the electronic structure and its potential to help understanding the properties of the materials in many other applications.

ASSOCIATED CONTENT

Supporting Information:

Supporting Information Available: The hematite sample thickness and measurement method (Table S1), PEC performance characterizations of the hematite films synthesized by different methods (Figure S1),O K-edge XAS of the sample substrate (Figure S2), comparisons between the TEY and TFY signals of the hematite films synthesized by different methods (Figure S3), detailed fittings of O K-edge TEY-XAS spectra (Figure S4) and TFY-XAS spectra

(Figure S5) of hematite films synthesized by different methods, Fe L-edge TEY-XAS spectra (Figure S6) and Fe L-edge RIXS spectra (Figure S7) and Fe L-edge Nr-XAS spectra (Figure S8) of the hematite films synthesized by different methods. The supporting information is available free of charge on the ACS Publication Website http://pubs.acs.org.

AUTHOR INFORMATION

Corresponding authors:

*jguo@lbl.gov

Notes

The authors declare no competing financial interests.

ACKNOWLEDGEMENTS

~~Acknowledgments:~~ The Advanced Light Source is supported by the Director, Office of Science, Office of Basic Energy Sciences, of the U.S. Department of Energy under Contract No. DE-AC02-05CH11231. D.W. gratefully thank the support from NSF (DMR 1055762). J. T. greatly thank the support from DOE SCGSR Fellowship and the ALS Doctoral Fellowship.

~~References~~REFERENCES:

1. Fujishima, A.; Honda, K., Electrochemical Photolysis of Water at a Semiconductor Electrode. *Nature* **1972**, *238*, 37-38.
2. Kapilashrami, M.; Zhang, Y.; Liu, Y.-S.; Hagfeldt, A.; Guo, J., Probing the Optical Property and Electronic Structure of Tio2 Nanomaterials for Renewable Energy Applications. *Chemical Reviews* **2014**, *114*, 9662-9707.
3. Lewis, N. S., Toward Cost-Effective Solar Energy Use. *Science* **2007**, *315*, 798-801.
4. Jing, D.~~;~~ Guo, L.; Zhao, L.; Zhang, X.; Liu, H.; Li, M.; Shen, S.; Liu, G.; Hu, X.; Zhang, X., et al., Efficient Solar Hydrogen Production by Photocatalytic Water Splitting: From Fundamental Study to Pilot Demonstration. *International Journal of Hydrogen Energy* **2010**, *35*, 7087-7097.
5. Maeda, K.; Domen, K., New Non-Oxide Photocatalysts Designed for Overall Water Splitting under Visible Light. *The Journal of Physical Chemistry C* **2007**, *111*, 7851-7861.
6. Reece, S. Y.; Hamel, J. A.; Sung, K.; Jarvi, T. D.; Esswein, A. J.; Pijpers, J. J. H.; Nocera, D. G., Wireless Solar Water Splitting Using Silicon-Based Semiconductors and Earth-Abundant Catalysts. *Science* **2011**, *334*, 645-648.
7. Maeda, K.; Teramura, K.; Lu, D.; Takata, T.; Saito, N.; Inoue, Y.; Domen, K., Photocatalyst Releasing Hydrogen from Water. *Nature* **2006**, *440*, 295-295.
8. Luo, J.; Im, J.-H.; Mayer, M. T.; Schreier, M.; Nazeeruddin, M. K.; Park, N.-G.; Tilley, S. D.; Fan, H. J.; Grätzel, M., Water Photolysis at 12.3% Efficiency Via Perovskite Photovoltaics and Earth-Abundant Catalysts. *Science* **2014**, *345*, 1593-1596.
9. Khaselev, O.; Turner, J. A., A Monolithic Photovoltaic-Photoelectrochemical Device for Hydrogen Production Via Water Splitting. *Science* **1998**, *280*, 425-427.
10. Jang, J.-W~~,~~,; Du, C.; Ye, Y.; Lin, Y.; Yao, X.; Thorne, J.; Liu, E.; McMahon, G.; Zhu, J.; Javey, A., et al., Enabling Unassisted Solar Water Splitting by Iron Oxide and Silicon. *Nature Communcations* **2015**, *6*, 7447.

279 11. Liu, C.; Dasgupta, N. P.; Yang, P., Semiconductor Nanowires for Artificial Photosynthesis. *Chemistry of*
280 *Materials* **2014**, *26*, 415-422.
281 12. Park, Y.; McDonald, K. J.; Choi, K.-S., Progress in Bismuth Vanadate Photoanodes for Use in Solar Water
282 Oxidation. *Chemical Society Reviews* **2013**, *42*, 2321-2337.
283 13. Chen, X.; Mao, S. S., Titanium Dioxide Nanomaterials: Synthesis, Properties, Modifications, and
284 Applications. *Chemical Reviews* **2007**, *107*, 2891-2959.
285 14. Mayer, M. T.; Lin, Y.; Yuan, G.; Wang, D., Forming Heterojunctions at the Nanoscale for Improved
286 Photoelectrochemical Water Splitting by Semiconductor Materials: Case Studies on Hematite. *Accounts of Chemical*
287 *Research* **2013**, *46*, 1558-1566.
288 15. Hamann, T. W., Splitting Water with Rust: Hematite Photoelectrochemistry. *Dalton Transactions* **2012**, *41*,
289 7830-7834.
290 16. Sivula, K.; Le Formal, F.; Grätzel, M., Solar Water Splitting: Progress Using Hematite (α-Fe_2O_3)
291 Photoelectrodes. *ChemSusChem* **2011**, *4*, 432-449.
292 17. Tamirat, A. G.; Rick, J.; Dubale, A. A.; Su, W.-N.; Hwang, B.-J., Using Hematite for Photoelectrochemical
293 Water Splitting: A Review of Current Progress and Challenges. *Nanoscale Horizons* **2016**, *1*, 243-267.
294 18. Du, C.; Zhang, M.; Jang, J.-W.; Liu, Y.; Liu, G.-Y.; Wang, D., Observation and Alteration of Surface States
295 of Hematite Photoelectrodes. *The Journal of Physical Chemistry C* **2014**, *118*, 17054-17059.
296 19. Lin, F.; Boettcher, S. W., Adaptive Semiconductor/Electrocatalyst Junctions in Water-Splitting
297 Photoanodes. *Nature Materials* **2014**, *13*, 81-86.
298 20. Thorne, J. E.; Li, S.; Du, C.; Qin, G.; Wang, D., Energetics at the Surface of Photoelectrodes and Its
299 Influence on the Photoelectrochemical Properties. *The Journal of Physical Chemistry Letters* **2015**, *6*, 4083-4088.
300 21. Smith, R. D. L.; Prévot, M. S.; Fagan, R. D.; Zhang, Z.; Sedach, P. A.; Siu, M. K. J.; Trudel, S.;
301 Berlinguette, C. P., Photochemical Route for Accessing Amorphous Metal Oxide Materials for Water Oxidation
302 Catalysis. *Science* **2013**, *340*, 60-63.
303 22. Thorne, J. E.; Jang, J.-W.; Liu, E. Y.; Wang, D., Understanding the Origin of Photoelectrode Performance
304 Enhancement by Probing Surface Kinetics. *Chemical Science* **2016**, *7*, 3347-3354.
305 23. Ye, Y.; Kawase, A.; Song, M.-K.; Feng, B.; Liu, Y.-S.; Marcus, M. A.; Feng, J.; Fang, H.; Cairns, E. J.;
306 Zhu, J., et al., X-Ray Spectroscopies Studies of the 3d Transition Metal Oxides and Applications of Photocatalysis. *MRS Communications* **2017**, *7*, 53-66.
307 24. Guo, J., Synchrotron Radiation, Soft-X-Ray Spectroscopy and Nanomaterials. *International Journal of*
308 *Nanotechnology* **2004**, *1*, 193-225.
309 25. Ye, Y.; Kawase, A.; Song, M.-K.; Feng, B.; Liu, Y.-S.; Marcus, M. A.; Feng, J.; Fang, H.; Cairns, E. J.;
310 Zhu, J., et al., X-Ray Absorption Spectroscopic Characterization of the Synthesis Process: Revealing the Interactions
311 in Cetyltrimethylammonium Bromide-Modified Sulfur–Graphene Oxide Nanocomposites. *The Journal of Physical*
312 *Chemistry C* **2016**, *120*, 10111-10117.
313 26. Liu, Y.-S.; Glans, P.-A.; Chuang, C.-H.; Kapilashrami, M.; Guo, J., Perspectives of in Situ/Operando
314 Resonant Inelastic X-Ray Scattering in Catalytic Energy Materials Science. *Journal of Electron Spectroscopy and*
315 *Related Phenomena* **2015**, *200*, 282-292.
316 27. Kronawitter, C. X.; Zegkinoglou, I.; Shen, S.-H.; Liao, P.; Cho, I. S.; Zandi, O.; Liu, Y.-S.; Lashgari, K.;
317 Westin, G.; Guo, J., et al., Titanium Incorporation into Hematite Photoelectrodes: Theoretical Considerations and
318 Experimental Observations. *Energy & Environmental Science* **2014**, *7*, 3100-3121.
319 28. Liang, Y.; Vinson, J.; Pemmaraju, S.; Drisdell, W. S.; Shirley, E. L.; Prendergast, D., Accurate X-Ray
320 Spectral Predictions: An Advanced Self-Consistent-Field Approach Inspired by Many-Body Perturbation Theory.
321 *Physical Review Letters* **2017**, *118*, 096402.
322 29. Gilbert, B.; Katz, J. E.; Denlinger, J. D.; Yin, Y.; Falcone, R.; Waychunas, G. A., Soft X-Ray Spectroscopy
323 Study of the Electronic Structure of Oxidized and Partially Oxidized Magnetite Nanoparticles. *The Journal of*
324 *Physical Chemistry C* **2010**, *114*, 21994-22001.
325 30. Kronawitter, C. X.; Bakke, J. R.; Wheeler, D. A.; Wang, W.-C.; Chang, C.; Antoun, B. R.; Zhang, J. Z.;
326 Guo, J.; Bent, S. F.; Mao, S. S., et al., Electron Enrichment in 3d Transition Metal Oxide Hetero-Nanostructures.
327 *Nano Letters* **2011**, *11*, 3855-3861.

31. Gilbert, B.; Frandsen, C.; Maxey, E. R.; Sherman, D. M., Band-Gap Measurements of Bulk and Nanoscale Hematite by Soft X-Ray Spectroscopy. *Physical Review B* **2009**, *79*, 035108.
32. de Groot, F. M. F.; Grioni, M.; Fuggle, J. C.; Ghijsen, J.; Sawatzky, G. A.; Petersen, H., Oxygen 1s X-Ray-Absorption Edges of Transition-Metal Oxides. *Physical Review B* **1989**, *40*, 5715-5723.
33. Suntivich, J.; Hong, W. T.; Lee, Y.-L.; Rondinelli, J. M.; Yang, W.; Goodenough, J. B.; Dabrowski, B.; Freeland, J. W.; Shao-Horn, Y., Estimating Hybridization of Transition Metal and Oxygen States in Perovskites from O K-Edge X-Ray Absorption Spectroscopy. *The Journal of Physical Chemistry C* **2014**, *118*, 1856-1863.
34. Shen, S.; Zhou, J.; Dong, C.-L.; Hu, Y.; Tseng, E. N.; Guo, P.; Guo, L.; Mao, S. S., Surface Engineered Doping of Hematite Nanorod Arrays for Improved Photoelectrochemical Water Splitting. *Scientifc Reports* **2014**, *4*, 6627.
35. Luo, K.;~~,~~ Roberts, M. R.; Hao, R.; Gurrini, N.; Picjup, D. M.; Liu, Y.-S.; Edstrom, K.; Guo, J.; Chadwick, A. V.; Duda, L. C., et al., Charge-Compensation in 3d-Transition-Metal-Oxide Intercalation Cathodes through the Generation of Localized Electron Holes on Oxygen. *Nature Chemistry* **2016**, *8*, 684-691.
36. Barbiellini, B.;~~,~~ Suzuli, K.; Orikasa, Y.; Kaprzyk, S.; Itou, M.; Yamamoto, K.; Wang, Y. J.; Hafiz, H.; Yamada, R.; Uchimoto, Y., et al., Identifying a Descriptor for D-Orbital Delocalization in Cathodes of Li Batteries Based on X-Ray Compton Scattering. *Applied Physics Letters* **2016**, *109*, 073102.
37. Vayssieres, L.; Sathe, C.; Butorin, S. M.; Shuh, D. K.; Nordgren, J.; Guo, J., One-Dimensional Quantum-Confinement Effect in A-~~Fe2o3~~ Fe2O3 Ultrafine Nanorod Arrays. *Advanced Materials* **2005**, *17*, 2320-2323.

TOC GRAPHICS